

INSTRUMENTS AND METHODS OF INVESTIGATION

PACS numbers: 96.50.Ek, 96.50.Zc, 96.60.Vg

Methods of local interstellar medium investigation

V G Kurt, E N Mironova

DOI: 10.3367/UFNe.0183.201309e.0963

Contents

Abstract. **The question of the Sun's motion relative to the local interstellar medium (LISM) is examined. Results from Russian, US, and French satellites and space probes observing scattered solar radiation in hydrogen Lyman-alpha ($\lambda = 1215.7$ Å) and helium ($\lambda = 584$ Å) lines are presented. Data are briefly discussed on the direct registration inside the Solar System of neutral helium atoms, picked-up helium ions, and fast neutral hydrogen atoms entering from the LISM. The fast neutral hydrogen atoms arise in the region of solar wind–LISM interaction.**

1. Introduction

In the 1960s, measurements in the upper atmosphere of the Earth, and later in interplanetary space, have culminated in the discovery of the phenomenon of interstellar wind (ISW) — the motion of the Sun relative to the surrounding local interstellar medium (LISM) [1–5]. At the same time, the theory of the solar wind's interaction with the incoming interstellar gas flow was elaborated [6]. A schematic layout of this interaction is presented in Fig. 1. The solar wind, which has a velocity of about 400 km s^{-1}, must collide with the interstellar medium charged component. According to paper [6], the interface resulting from this collision consists of two shocks, between which the separation boundary between heated and stopped solar wind particles and the interstellar medium, the heliopause, is located. The region inside the first bow shock dominated by the solar wind is called the heliosphere. The interstellar medium surrounding the solar system outside the second shock is thought to be unperturbed. Recently, the existence of the external bow shock has been put in doubt [7].

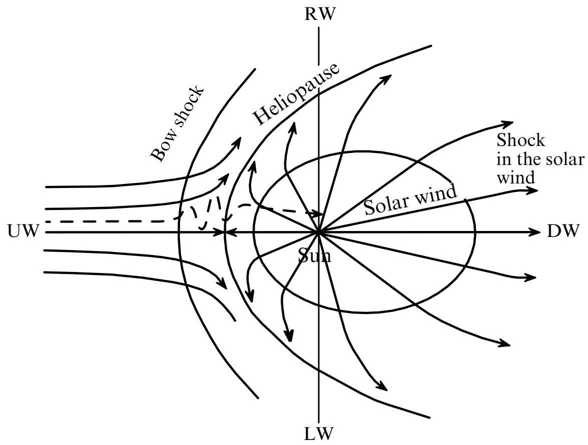

Figure 1. General scheme of the solar wind's interaction with the interstellar medium: DW — downwind direction; UW — upwind direction; LW and RW — directions normal to the UW–DW line.

According to the classical theory, the so-called Stromgren zone should exist around the Sun with a size of ~ 1200 astronomical units (A.U.), inside which matter should be fully ionized. The motion of the Sun relative to the ISM radically changes the picture: neutral LISM components freely penetrate the heliospheric interface and can be directly observed [8]. Their detection and subsequent interpretation allow the unperturbed LISM parameters to be determined.

2. Ultraviolet studies of the interstellar medium and local interstellar medium

Neutral interstellar atoms which entered the heliosphere are subjected to gravitational attraction and interact with

V G Kurt, E N Mironova Astro Space Center,
Lebedev Physical Institute, Russian Academy of Sciences,
Leninskii prosp. 53, 119991 Moscow, Russian Federation
Tel. + 7 (495) 333 23 33. Fax + 7 (495) 333 23 78
E-mail: vkurt@asc.rssi.ru

Received 5 July 2012, revised 2 October 2012
Uspekhi Fizicheskikh Nauk **183** (9) 963 – 972 (2013)
DOI: 10.3367/UFNr.0183.201309e.0963
Translated by K A Postnov; edited by A Radzig

corpuscular and electromagnetic radiations from the Sun, causing changes in the trajectories and physical state of the atoms. As a result, a certain distribution of neutral atoms penetrated from the LISM is established inside the Solar System at every instant of time. These are, first of all, atoms of neutral hydrogen and helium, which manifest themselves due to resonance scattering of the solar L_α-emission (the wavelength $\lambda = 1215.7$ Å) and He I ($\lambda = 584$ Å) emission. Initially, the ground-state electrons in such atoms absorb solar radiation quanta with wavelength $\lambda = 1215.7$ Å (584 Å for helium), rise to the first excited level, and then return to the ground state by emitting quanta with the corresponding wavelength.

The L_α-emission from ISM hydrogen atoms was first detected in the interplanetary space by the *Zond-1* spacecraft [2]. The registration scheme was very simple. A Geiger counter filled with NO and a 2-mm window made of lithium fluoride (LiF) in the first channel and calcium fluoride (CaF_2) in the second channel was utilized as the detector. The short-wavelength spectral sensitivity was limited by the window transmission at $\lambda = 1050$ Å for LiF and at $\lambda = 1225$ Å for CaF_2. The long-wavelength sensitivity boundary was determined by the nitrogen oxide ionization potential of 9.23 eV ($\lambda = 1340$ Å). Thus, the first counter measured the total intensity in the L_α line and the atomic oxygen triplet ($\lambda = 1302$, 1304, and 1305 Å), while the counter with the CaF_2 window measured only the intensity of the atomic oxygen triplet.

Later on, the simple filters were substituted by a more advanced cell filter allowing measurement of both the L_α-emission and the scattered line profile. The examination of this profile under certain assumptions enables the temperature of the interstellar hydrogen, as well as three components of the Sun's velocity relative to the LISM, to be measured. Cell filters were employed in studying the L_α-emission aboard *Mars-6* and *Atlas-1* spacecraft, on the satellites *Prognoz-5* and *Prognoz-6*, and aboard the solar observatory SOHO (SOlar and Heliospheric Observatory) in the SWAN (Solar Wind ANisotropies) detector.

Figure 2 depicts the optical scheme of the L_α-emission measurement channels of photometers installed on the satellites *Prognoz-5* and *Prognoz-6* [9]. Photo-electron multipliers (PMs) were utilized as detectors. A small hermetic glass vessel with walls covered from inside by teflon (fluoroplastic) and two MgF_2 windows found use as an absorption cell. In the input window, a lens focused between the cell and PM was installed. The rectangular window restricted the space to a $1.3° \times 3.0°$ field of view in the focal plane. A thin film selecting a 10-nm band centered on the L_α line was evaporated onto the output window. The preliminarily vacuumized cell was filled with molecular hydrogen mixed with inert xenon. When the cell was switched on, the electric current flowed through a tungsten wire inside the cell (sometimes two wires were used) and heated it up, and a dissociation of hydrogen molecules occurred. As a result, atomic hydrogen with an optical depth τ proportional to the strength of the current flowing through the cell emerged. About 0.05 s after switching off the current, the complete recombination of atomic hydrogen into molecular hydrogen occurred. The cell filled with molecular hydrogen was fully transparent to the L_α-emission (of course, taking into account the window transmission). When atomic hydrogen appeared inside the cell, part of the photons with a frequency close to the resonance line center were scattered and absorbed by the cell walls. The ratio of the sensor indication with a switched-on cell to that with a switched-off cell is called the factor reduction (FR).

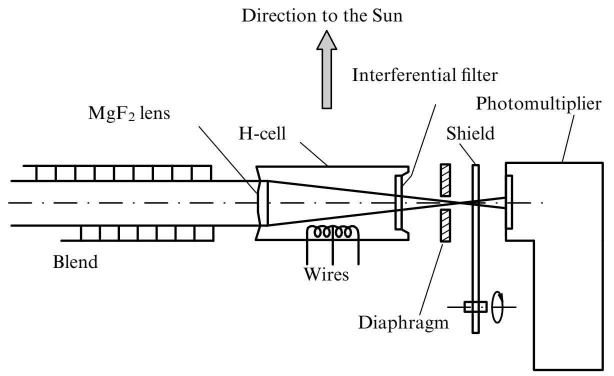

Fiure. 2. Optical scheme of the L_α-channel.

The theory of a hydrogen absorption cell is presented in detail in paper [10]. The optimal optical depth for interplanetary L_α-emission studies is found to be $\tau \approx 10$.

High-resolution ultraviolet (UV) GHRSs (Goddard High-Resolution Spectrographs) and STISs (Space Telescope Imaging Spectrographs) aboard the Hubble Space Telescope (HST) were also tapped in studying the interplanetary L_α-emission line profile [11–13].

To register emission from He atoms, channel electron multipliers serve as detectors. In the latter, thin metallic (Al or Sn) filters (with a thickness of a few hundred angstroms) are used as windows of a cell (if it is used), and the optical depth is controlled by the amount of helium pumped into the cell [14, 15].

2.1 Ultraviolet observations of neutral hydrogen and local interstellar medium parameters

The only quantity which can be measured in L_α line observations is the volume emission integrated along the line of sight. For theoretical reconstruction of the observed emission, some parameters which characterize the interstellar wind proper and some solar parameters must be known. To calculate the number density $n(r, \theta)$ of neutral hydrogen atoms in the Solar System as a function of r, the distance to the Sun, and θ, the angle with a vertex in the Sun that is included between the upwind direction and the line of sight from a given point, it is necessary to know the value and the direction of the velocity vector $\mathbf{V}_w$ (V_w, α_w, δ_w) and the temperature T_w of hydrogen atoms at infinity. The number density n_∞ of hydrogen atoms at infinity is calculated separately and requires the absolute laboratory calibration of the detector, i.e., the conversion of detector's pulse rate (counts per s) to intensity units (in erg cm^{-2} sr^{-1} s^{-1}) (see the Appendix).

The trajectories of hydrogen atoms in the interstellar wind flowing into the Solar System are changed due to the solar gravitational attraction force F_G and the repulsion force F_R caused by radiation pressure in the L_α line. The ratio $\mu = F_R/F_G$ is used in calculations. The solar radiation pressure force is directly related to the emission intensity F_s in the center of a solar L_α line measured in units of photons per cm^2 per s per Å.

There is a large probability that a hydrogen atom will be ionized when moving toward the Sun. Closer to the Sun, the degree of ionization increases, and a cavity containing virtually no atomic hydrogen is formed. The form and size of the cavity also depend on the relation between the gravitational force and radiation pressure in the L_α line. The ionization rate $1/\tau$ [s^{-1}] of atomic hydrogen is determined by the relation $1/\tau = 1/\tau_{sw} + 1/\tau_{euv}$, where $1/\tau_{sw}$ is the ionization rate by the solar wind due to charge exchange reactions of solar wind protons with neutral hydrogen atoms, and $1/\tau_{euv}$ is the ionization rate by solar hard ultraviolet ($\lambda < 912$ Å) and X-ray radiation .

Thus, the following parameters: T_w, $\mathbf{V}_w$ (V_w, α_w, δ_w), μ, and $1/\tau$ should be determined from the observed intensity along the line of sight. Unfortunately, it is impossible to derive analytical formulae for the observed emission line intensity. As the interstellar gas temperature is about 10,000 K, the thermal velocity of atoms is sufficient, by order of magnitude, to deflect the direction of motion of many atoms from vector $\mathbf{V}_w$. As a result, the density of atoms in each element of space inside the heliosphere is determined by all atoms coming from some volume of the velocity space (the 'hot' model).

The starting point of calculations in the hot model is the assumption that all atoms move with one velocity $\mathbf{V}_w$ before interacting with the Sun (the 'cold' model). Depending on μ ($\mu < 1$ or $\mu > 1$), the trajectories of atoms affected by the Sun will differ greatly (Fig. 3). (Here, heliocentric polar coordinates in the plane formed by the group velocity vector $\mathbf{V}_w$ and the considered point $M(r, \theta)$ are used.)

For $\mu < 1$, the volume emissivity at the point $M(r, \theta)$ has the form [16, 17]

$$\varepsilon_{cold}(r, \theta, V) = n_\infty g_0 (n_1 m_1 \Phi_1 + n_2 m_2 \Phi_2)\,,$$

where n_∞ is the LISM particle number density before interaction with the heliosphere (number of atoms per cm^3),

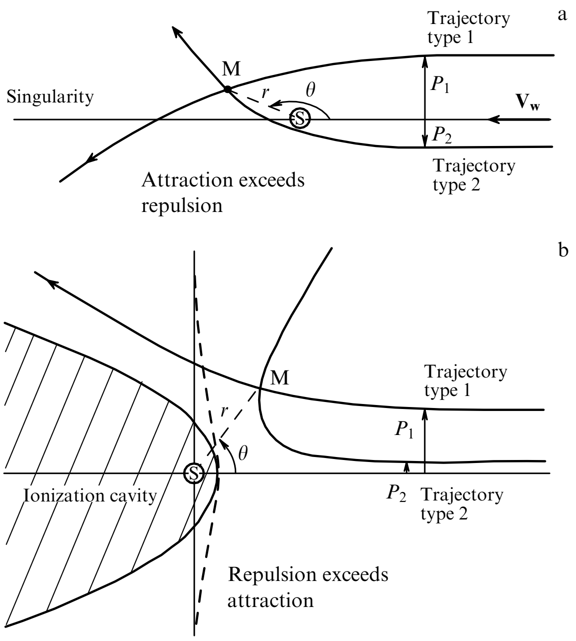

Figure 3. Cold model geometry: (a) $\mu < 1$, and (b) $\mu > 1$. Atoms moving along two hyperbolic trajectories with impact parameters P_1 and P_2 come from infinity to point M with polar coordinates (r, θ). For $\mu < 1$ there are two types of trajectories. If the angle $\theta \leqslant \pi$, the trajectory is 'straight'; if $\theta > \pi$, the trajectory is 'not straight.' The density of atoms becomes indefinite on the S–DW-axis (S denotes the Sun). For $\mu > 1$, only straight trajectories exist. The size of the cavity that is free from neutral hydrogen depends on the velocity $\mathbf{V}_w$ and μ. The density becomes indefinite on the parabolic surface of the cavity.

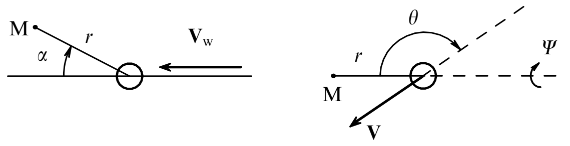

Figure 4. Hot model geometry. At point M with polar coordinates (r, α), where α is the angle between the direction from the Sun to the point M and the DW direction, the cold model densities should be integrated in the velocity space at infinity over the module $\mathbf{V}$ and angles θ and ψ.

g_0 is the excitation factor — the number of photons scattered by an atom at rest at a distance of 1 A.U. into the solid angle 4π sr per second, n_1, n_2 are the number density of atoms coming into point M along trajectories 1 and 2, m_1, m_2 are the losses inflicted by ionization during the movement toward point M along trajectories 1 and 2, respectively, and Φ_1, Φ_2 are the relative photon fluxes incident on the atom.

Figure 4 illustrates the geometry of the hot model. The point M has spherical coordinates (r, θ). For the Maxwell–Boltzmann distribution, the fraction of atoms at the point $M(r, \alpha)$ possessing the velocity $\mathbf{V}$ (V, θ, ψ) at infinity is given by

$$dn = \left(\frac{m}{2\pi k_B T}\right)^{3/2} \exp\left(-\frac{mW^2}{2k_B T}\right) V^2\,dV \sin\theta\,d\theta\,d\Psi\,,$$

where m is the hydrogen atom mass, T is the unperturbed gas temperature, k_B is the Boltzmann constant, and $\mathbf{W}$ is the individual thermal velocity of an atom: $\mathbf{V} = \mathbf{V}_w + \mathbf{W}$.

The calculation of the volume emissivity ε_{hot} in the hot model is reduced to the calculation of the triple integral in the velocity space:

$$\varepsilon_{hot}(r, \alpha) = \iiint \varepsilon_{cold}(r, \theta, \mathbf{V})\,dn\,.$$

The 'classical' hot model described above assumes that the solar radiation is isotropic and stationary. The solar L_α line near the maximum is considered to be flat. The optically thin approximation is applied. It is also assumed that the distribution of neutral atoms penetrated into the heliosphere is symmetric with respect to the upwind–downwind (UW–DW) axis. The best-fit parameters are found by comparing observational results with the theoretical volume emissivities integrated along the line of sight. If we wish to seek all seven parameters, five of which characterize the LISM properties and two of which relate to the Sun, the determination accuracy will be rather poor. In addition, agreement with observations can be achieved for different sets of the parameters sought after [9], because of deviations from the assumptions adopted in 'classical' model.

At $\mu = 1$, neutral hydrogen atoms move along straight trajectories, and their density depends only on the ionization process (the model of 'straight' trajectories).

Observations made by the *Prognoz-5* and *Prognoz-6* satellites also showed for the first time that the solar wind tends to weaken in the direction from the equator to the poles of the Sun [18]. This leads to asymmetry of ionization processes involving charge exchange of neutral hydrogen atoms with solar wind protons. The situation becomes more complicated due to the presence of secondary flows of hydrogen and helium atoms emerging at the heliospheric boundary [19, 20]. With a velocity of ~ 20 km s^{-1}, the time it takes for atoms to pass through the heliosphere reaches several dozen years. Therefore, parameters derived from the UV observations represent, in fact, values averaged over the last several years.

Despite these difficulties, the classical model in some cases provides a sufficiently good approximation, especially if it is possible to restrict the number of parameters being sought. For example, the analysis of the *Prognoz-5* and *Prognoz-6* observational results revealed that the FR curves are quite sensitive to parameters μ, T, and $\mathbf{V}_{\rm w}$ [9]. This allows one, by fixing μ and the direction of $\mathbf{V}_{\rm w}$, to deduce quite accurately the temperature and velocity from FR curves. In this regard, the best fit was obtained only when observations for the upwind and downwind hemispheres were processed separately. The results obtained for the upwind hemisphere are preferable since, in this case, the incident flux of hydrogen atoms has not been strongly perturbed yet, in contrast to the downwind flux, which has already experienced stronger perturbations by flying past the Sun.

The number of the parameters sought can be reduced when some of them can be found independently. First of all, this relates to the direction of vector $\mathbf{V}_{\rm w}$. The first detailed L_α line observations by the *OGO-5* satellite [1] in 1970 already revealed a parallactic shift of the L_α line intensity maximum caused by the scattering on neutral hydrogen atoms located within 10 A.U. from the Sun [4, 6].

There are four special directions in the Solar System, along which observations enable independent measurement of certain parameters (see Fig. 1). These include, first of all, the upwind (UW) and downwind (DW) directions, along which the maximum and minimum intensities of the L_α line should be observed, respectively. Observations in the diametrically opposite directions (RW and LW), which are normal to the UW–DW axis, must yield similar results. The use of these features depends on the geometry of observations in each specific experiment. For example, in the *Prognoz-5* and *Prognoz-6* observations, when the axis of the detector registering L_α-emission scanned large circles tangent to Earth's orbit, the same RW and LW intensities implied that Earth's longitude at this moment was equal to UW or DW (the independent determination of $\lambda_{\rm w}$).

The use of a hydrogen absorption cell and the determination of the factor reduction proved to be powerful tools for probing the temperature and velocity of motion of the LISM. The angular Doppler spectral scanning method allows measurement of $T_{\rm w}$ and $\mathbf{V}_{\rm w}$ (the absolute value and direction) to be made, both for the all-sky survey and for the observational mode utilized by the *Prognoz-5* and *Prognoz-6* satellites, when it was sufficient to perform three scanning circles to determine these values [10]. At infinity, hydrogen atoms were assumed to have isotropic Maxwell velocity distribution which was preserved in the interplanetary space, too. This assumption is justified by the condition $\mu \approx 1$ and the absence of a galactic background.

The factor reduction can be expressed as a function of the Doppler shift $\Delta\lambda_{\rm D}$ in the following way:

$$\mathrm{FR}(\Delta\lambda_{\rm D}) = \frac{I(\Delta\lambda_{\rm D})}{I_0} = \frac{\int f(\lambda - \Delta\lambda_{\rm D})\, T(\lambda)\,\mathrm{d}\lambda}{\int f(\lambda)\,\mathrm{d}\lambda}\,.$$

Here, $I(\Delta\lambda_{\rm D})$ is the observed intensity in the presence of a radial velocity leading to the Doppler shift $\Delta\lambda_{\rm D}$; I_0 is the observed intensity at $\Delta\lambda_{\rm D} = 0$; $f(\lambda)$ is the emission line profile, and $T(\lambda)$ is the cell transmission as a function of wavelength: $T(\lambda) = \exp(-\tau H(a, v))$, where τ is the optical depth, $a = 2.7 \times 10^{-3}$ is the ratio of the natural line width to the Doppler width $\Delta\lambda_{\rm c} = (\lambda_{\rm c}/c)(2k_{\rm B}T_{\rm c}/m)^{1/2}$, $T_{\rm c}$ is the gas kinetic temperature in the cell, $v = (\lambda - \lambda_0)/\Delta\lambda_{\rm c}$, λ_0 is the line center wavelength, and $H(a, v)$ is the non-normalized Voigt function [21].

The Voigt profile appears when Gaussian (Doppler) and Lorentzian line broadening operate in statistically independent ways. In the cell, the Gaussian profile near the line center is added to the Lorentzian wings (due to damping, when $\Delta\lambda > 3\Delta\lambda_{\rm D}$).

For the Gaussian profile of the interplanetary L_α line, corresponding to temperature $T_{\rm e}$, the factor reduction can be presented in an integral form as a function of $T_{\rm e}$, $V_{\rm D}$, and τ:

$$\mathrm{FR}(T_{\rm e}, V_{\rm D}, \tau) = \frac{1}{\Delta\lambda_{\rm e}\sqrt{\pi}} \int_{-\infty}^{\infty} \exp\left[-\frac{(\Delta\lambda_{\rm D} - \Delta\lambda)^2}{\Delta\lambda_{\rm e}^2} - \tau H(a, v)\right] \mathrm{d}\lambda\,,$$

where $\Delta\lambda_{\rm e} = (\lambda_0/c)(2k_{\rm B}T_{\rm e}/m)^{1/2}$, and $\Delta\lambda = \lambda - \lambda_0$.

Figure 5 illustrates the operation principle of the absorption cell with $\tau = 10$ and the temperature inside the cell $T_{\rm c} = 300$ K at $V_{\rm D} = 0$ and $V_{\rm D} = 10$ km s^{-1} ($V_{\rm D}$ is the velocity leading due to the Doppler shift). The emission line has a Gaussian profile corresponding to the temperature 15,000 K.

Figure 6 depicts the factor reduction for the Gaussian profile as a function of temperature for different Doppler shifts [9]. From the $\mathrm{FR}_{\min}$ curve at $V_{\rm D} = 0$ one can determine $T_{\rm w}$.

To date, the most complete observations in the L_α line have been made with the SWAN instrument aboard the *SOHO* solar observatory [22–25]. Already during the first year of observations, the space distribution of visible velocities across the entire sky but a region located 5° away from the ecliptic pole was obtained. The dependence of the interplanetary L_α-emission and solar wind anisotropy on the solar activity cycle was examined.

A new estimate of the upwind direction has been made: $\lambda_{\rm w} = 252° \pm 0.73°$, and $\beta_{\rm w} = 8.7° \pm 0.90°$ (ecliptic coordi-

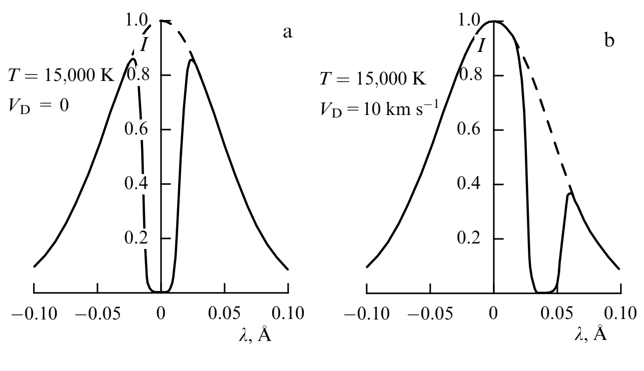

Figure 5. Effect of absorption by a cell with $r = 10$ and temperature $T_{\rm c} = 300$ K of a line with the Gaussian profile corresponding to a temperature of 15,000 K, for velocities producing the Doppler shift (a) $V_{\rm D} = 0$ and (b) $V_{\rm D} = 10$ km s^{-1}. The dashed and solid lines show the line profiles before and after absorption, respectively [10]. The intensity I is given in relative units.

[1] Abbreviation from Orbiting Geophysical Observatory.

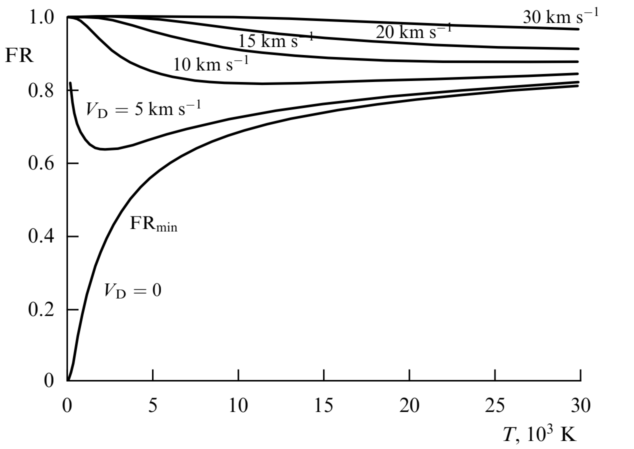

Figure 6. Factor reduction (FR) for the Gaussian line profile as a function of temperature for different Doppler shifts shown alongside the curves. The FR$_{min}$-curve allows the temperature of emitting hydrogen to be determined from FR measured at a zero Doppler shift [10].

nates, epoch J2000.0). The difference between this finding and the results obtained from helium observations (see Section 2.2) by $3^\circ - 4^\circ$ can be related, according to paper [23], to an asymmetry of the heliosphere caused by the interstellar magnetic field. The velocity difference between the upwind and downwind directions at the time of observations (1996–1997) allowed calculation in the frame of the classical hot model of the relation between the solar radiation pressure in the L_α line and the gravitational attraction force from the Sun, $\mu = 0.9 - 1.0$, and of the velocity of hydrogen atoms ranging 21–22 km s^{-1}. The velocity obtained is related to the region distant by ~ 50 A.U. from the Sun. Thus, hydrogen atoms slow down in the interaction region between the solar wind and the interstellar medium by 2.5–4.5 km s^{-1}.

Using observational data obtained directly with the aid of a hydrogen absorption cell, the temperature variation along the line of sight was measured as a function of the angle between the line of sight and the interstellar wind direction [22]. A temperature minimum was found between the upwind direction and the normal to it, while classical models predict a monotonic line-of-sight temperature increase from the upwind to the downwind direction. This implies the presence of two populations of interstellar atoms in the heliosphere with different velocities (primary and secondary populations), as predicted by the interaction models of the interstellar gas with the solar wind [24, 25]. If the spectral line broadening due to radiation transfer can be neglected, the obtained Maxwellian temperature of the incident hydrogen flux is within the range of 10,000–13,000 K, which suggests its heating in the ISM–solar wind interaction region.

2.2 Ultraviolet observations of neutral helium and local interstellar medium parameters

In 1973, a weak emission in the neural helium spectral line ($\lambda = 584$ Å) of interplanetary origin was discovered [26, 27]. Later on, observations from satellites and interplanetary probes were tapped to map the He I-line ($\lambda = 584$ Å) emission in wide sky areas [28–30].

There are some advantages facilitating the interpretation of He I-line observations, despite the fact that the intensity of emission in this helium line is two orders of magnitude weaker than that in the hydrogen L_α line. The interaction cross section of neutral helium atoms with solar wind protons is small and in consequence neutral helium atoms freely pass through the heliospheric interface region and take no ionization losses due to charge exchange reactions, which are so important for neutral hydrogen. The atomic helium ionization by hard ultraviolet and X-ray solar radiations is also insignificant. Helium atoms have a higher ionization potential compared to hydrogen atoms and penetrate much deeper inside the Solar System, so their concentration near Earth's orbit is significantly higher than that of hydrogen. In addition, it is possible to neglect the solar radiation pressure on helium atoms. Therefore, the distribution of neutral helium atoms in the Solar System is radically different from that of hydrogen atoms. The ionization cavity formed by solar ultraviolet and X-ray radiation is small in size and lies within Mercury's orbit, and atoms flying past the Sun are deflected by solar gravitational force to form the narrow cone observed, which allows the precise determination of the upwind direction. This was done for the first time from high-apogee satellites *Prognoz-5* and *Progrnoz-6*, whose detectors scanned the helium cone from Earth's orbital motion [17, 31].

Interesting results were also obtained by the American satellite *EUVE* (Extreme UltraViolet Explorer), which was

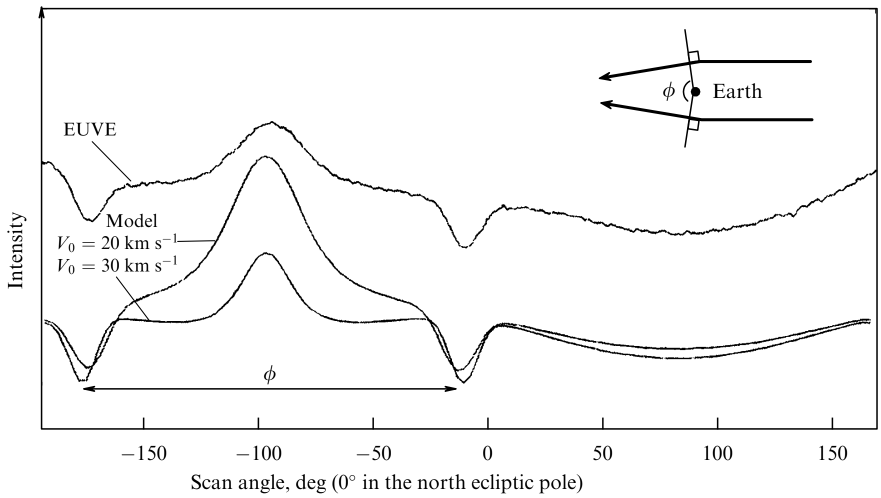

Figure 7. Interstellar wind velocity determination from *EUVE* observations [29].

placed in an orbit with an altitude of only 500 km [32]. Due to a low orbit, geocoronal helium emission in the line $\lambda = 584$ Å contributed significantly to the *EUVE* observations. On the other hand, geocoronal absorption lines provided information on the interstellar wind velocity, since their location in the scan circles depended on the difference between the ISW and Earth's velocity vectors. To illustrate this dependence, we show in Fig. 7 [32] one *EUVE* observation scan and two theoretical scans for the ISW velocities of 20 and 30 km s^{-1}. The geocorona operates as an absorption cell by producing maximum absorption when the projection of the velocity of helium atoms onto the line of sight vanishes in the Earth's rest frame. If there were no gravitational focusing of helium, the absorption maxima would be observed in two opposite directions normal to the original flux vector. The focusing decreases the angle between the directions of two absorption maxima, and its actual value depends on the helium flow velocity; therefore, the measurement of this angle provides an independent measurement of the ISW velocity.

Although *EUVE*'s orbit lay inside Earth's helium corona, data obtained by an antisolar photometer, which was in Earth's shadow at all times, provided the best measurements of the solar line width owing to the Doppler attenuation in the upwind direction. This line width was used in the subsequent interpretation of the observations.

The interpretation of helium line observations is somewhat simpler than that of the hydrogen line. It was shown that under the Maxwellian thermal velocity distribution of helium atoms at infinity (which is valid for a thermodynamically equilibrium medium), the triple integral for calculation of the atomic density along the cone axis in the hot model is reduced without loss of accuracy to a single integral, and one can apply the cold model with a sufficient accuracy beyond the part of the cone with $\theta > \theta_{\mathrm{cr}}$ [16, 33]. Here, the following notation was introduced:

$$\theta_{\mathrm{cr}} = \arctan \frac{(2k_{\mathrm{B}} T_{\mathrm{w}}/m_{\mathrm{He}})^{1/2}}{V_{\mathrm{w}}},$$

where m_{He} is the helium atom mass.

From observations of the interplanetary He I line ($\lambda = 584$ Å), the following LISM parameters were derived [32]:

— ecliptic coordinates of the downwind direction (J2000.0) $\lambda_{\mathrm{w}} = 74.7° \pm 0.5°$, $\beta_{\mathrm{w}} = -5.7° \pm 0.5°$;

— group velocity of helium atoms at infinity, $V_{\mathrm{w}} = 24.5 \pm 0.2$ km s^{-1};

— temperature $T_{\mathrm{w}} = 6500 \pm 2000$ K, and $n_{\mathrm{He}} = 0.013 \pm 0.003$ cm^{-3}.

3. Determining local interstellar medium parameters from direct detection of helium atoms in interplanetary space

Helium atoms were directly registered in the interplanetary space for the first time by the GAS (Ulysses Interstellar Neutral Gas) detector aboard the *Ulysses* spacecraft [34, 35]. Launched in 1990, the latter space probe began acquiring additional acceleration since 1992 under the action of gravitational attraction by Jupiter, and its ecliptical longitude started increasing and reached a maximum of 80.2° in September 1994.

The GAS instrument detected individual helium atoms and determined the direction of their motion. A rotating platform provided an almost complete sky survey. These data allowed measurements of the velocity vector, as well as temperature and density of neutral helium flux outside the heliosphere [34] under the following conditions:

— radiation pressure on helium atoms can be neglected;

— there is no charge exchange between helium atoms and solar wind protons;

— helium atoms move along Keplerian trajectories under the solar attraction.

In the GAS instrument, lithium fluoride was utilized as a detector. Secondary electrons and ions, which emerged in the collisions of helium atoms with LiF molecules, were ultimately detected by channel electron multipliers. Lithium fluoride is transparent to UV radiation, which precluded its influence on the measurement of L_α-emission. However, LiF is a very aggressive chemically; therefore, in order to keep transparency to UV radiation and the emission efficiency of secondary electrons, regular renovation of the surfaces of the detectors was needed, so that pure LiF was present. For this purpose, a special evaporation system was installed.

Interstellar helium atoms can come to a given point inside the heliosphere by moving along hyperbolic trajectories of two types (Fig. 8) lying in one plane whose position was determined by vector $\mathbf{V}_{\mathrm{w}}$ and the positions of the Sun and the observer. The kinetic energy of these particles (~ 10 eV) is close to the detector's sensitivity threshold, so a favorable combination of an atomic velocity vector and the spacecraft's velocity vector was required for an effective operation of the detector. For atoms moving along straight trajectories, this was possible from October 1990 to February 1992, and in the period from the end of 1994 to the beginning of 1995 it was possible to register atoms moving along both straight and not straight trajectories. Observations were carried out until August 1996 and then resumed from September 2000 until August 2002. Simultaneous observations of helium atoms moving along trajectories of both types permit direct determination of the contributions from photoionization

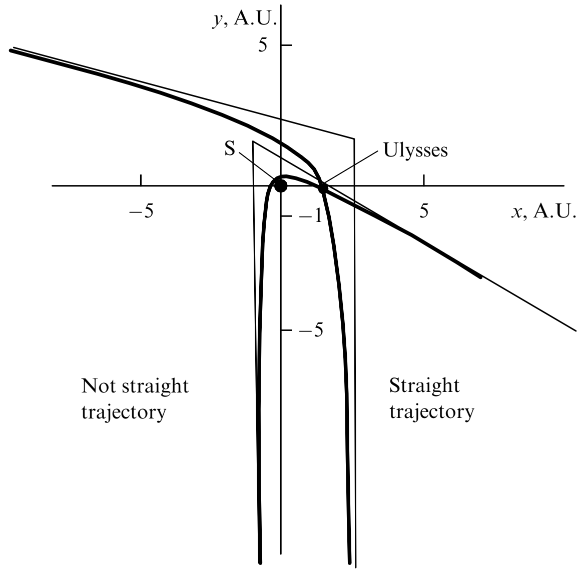

Figure 8. Straight and not straight hyperbolic trajectories of helium atoms which intersected the orbit of the *Ulysses* spacecraft located in perihelion in February 1995. Atoms resided in the not straight orbits (their degree of ionization reached 98%) approached the Sun much more close (by 0.2 A.U.) than those in the straight orbits. Simultaneous observations of fluxes of these particles were used to determine the rate of photoionization, which is the main source of losses.

and collisional ionization with high-energy solar wind electrons to the ionization of helium atoms.

As a result, more than 300 distributions of neutral helium atoms across the sky were measured. Averaged LISM parameters as derived from these observations are as follows:

— ecliptic coordinates of the downwind direction (J2000.0) $\lambda_{\rm w} = 74.7° \pm 0.5°$, $\beta_{\rm w} = -5.2° \pm 0.2°$;

— group velocity of helium atoms at infinity $V_{\rm w} = 26.3 \pm 0.4$ km s^{-1};

— temperature $T_{\rm w} = 6300 \pm 340$ K.

The method of reconstruction of the LISM parameters from the GAS observational data is described in more detail in Ref. [36].

The *IBEX* (Interstellar Boundary EXplorer) satellite launched in the USA on 19 October 2008 was equipped with instruments for direct registration in the interplanetary space of not only neutral helium atoms, but also hydrogen, neon, and oxygen atoms. The IBEX-Lo sensor [37] comprises a time-of-flight, triple-coincidence mass spectrometer. The results of this experiment are somewhat different from those obtained by the GAS instrument [38, 39]. The same situation, known as early as the time of processing and interpretation of UV observations of scattered L_α-emission, occurred: observations are consistent with different LISM parameters [40].

The LISM parameters selected from the results of IBEX-Lo measurements are as follows:

— ecliptic coordinates of the downwind direction (J2000.0) $\lambda_{\rm w} = 79.2°$, $\beta_{\rm w} = -5.12°$;

— group velocity of helium atoms at infinity $V_{\rm w} = 22.756$ km s^{-1};

— temperature $T_{\rm w} = 6165$ K.

4. Direct detection of local interstellar medium ions in the Solar System

The detection of so-called pick-up ions, which compose ionized LISM neutrals entrained by the solar wind inside the heliosphere, provides yet another way of studying LISM parameters. The first such experiments were carried out in the middle of the 1980s. The SULEICA (Suprathermal Energy Ionic Charge Analyzer) sensor aboard the *AMPTE/IRM* (Active Magnetospheric Particle Tracer Explorers/Ione Release Module) satellite scanned the cone formed by the helium ions focused behind the Sun twice. The mass spectrometer selected the incoming ions by their energy/charge ratio, then a spherical section analyzer carried out a time-of-flight analysis, and the residual energy of ions was measured with a silicon detector [41]. Five scans of the He^+ cone were obtained in 1998 from the *ACE* (Advanced Composition Explorer) satellite using the SWICS (Solar Wind Ion Composition Spectrometer) sensor [42]. Most of the data on the pick-up ions was obtained by the SWICS instrument aboard the *Ulysses* satellite — H^+, $^4He^{++}$, $^3He^+$, N^+, O^+, and Ne^+ ions were registered.

To compare theory with observations, the hot model was applied. The mean ionization rate of helium atoms was obtained from measurements of radio emission flux from the Sun at 10.7 cm, which correlates well with the solar UV radiation. The broadening of the cone with ionized atoms due to spatial diffusion and convection was taken into account. However, the accuracy of the results turned out to be low due to strong variations of the fluxes of the pick-up ions [44]. Nevertheless, SWICS/*Ulysses* estimated quite precisely the hydrogen density (0.1 cm^{-3}) and helium density (0.015 cm^{-3}) in the neighborhood of the heliospheric shock [42].

5. Study of the Solar System's edges

In 1977, two automatic interplanetary stations (AISs), *Voyager-1* and *Voyager-2* were launched by NASA/JPL (USA) for exploration of giant planets and their satellites. After crossing Pluto's orbit, both AISs started investigating remote parts of the Solar System. Presumably, the stations will be operational until 2020–2025. The successful flight of both spacecraft has been possible thanks to fully taking into account the experience obtained during *Pioneer-10* and *Pioneer-11* missions, which crossed the asteroid belt, reached Jupiter and Saturn, and probed the radiation situation near Jupiter. The last signal from *Pioneer-10*, which was at a distance of 80 A.U. from the Sun, was received in January 2003. The connection with *Pioneer-11* was disrupted in November 1995, when it was at a distance of ~ 45 A.U. from the Sun.

In December 2004, sensors aboard *Voyager-1* which was at a distance of 94 A.U. from the Sun at the time, signalled the crossing of the internal shock. This was the first experimental confirmation of a theory developed several decades ago [6]. *Voyager-2* first crossed the shock front on August 31, 2007 and crossed it again several times the next day, which suggested a nonstatic shock front. At that time, the spacecraft was 7–10 A.U. closer to the Sun than *Voyager-1* in December 2004. The revealed asymmetry of the heliosphere (compression of its southern hemisphere) is apparently due to the interstellar magnetic field pressure [45]. These results supported the conclusion about the asymmetry of the heliospheric shock inferred from numerical simulations of the region of an LISM interaction with the solar wind [46, 47].

In addition, *Voyager-2* space probe made another unexpected observation. Solar wind braking by the interstellar gas must have led to a sharp increase in the wind plasma density and temperature. Indeed, the temperature at the shock boundary turned out to be higher than in the inner heliosphere, but still only a tenth of what was expected. Data obtained by the plasma detector aboard *Voyager-2* showed that processes proceeding near the shock and in the adjacent regions are strongly affected by 'pick-up' (by the solar wind) ions — interstellar neutrals penetrating inside the heliosphere and being ionized there. By acquiring additional energy in the shock, the interstellar neutrals interact with incident neutrals of the interstellar wind and become atomic particles energetic enough to reach Earth's orbit [48]. Such neutrals were observed in 2007 from the *STEREO-A* and *STEREO-B*[2] satellites, which revolve around the Sun in Earth's orbit (artificial Trojan satellites of Earth) [49]. Neutral hydrogen atoms, dominating in the interstellar wind, mostly participate in these processes, especially in view of the large proton–hydrogen atom interaction cross section (amounting to a maximum of 1.5×10^{-15} cm^2 at an energy of 15 eV).

Complex and poorly understood processes in the shock and its vicinity complicate the transition to unperturbed LISM parameters. First and foremost, this relates to the hydrogen density and the LISM temperature determined from observations of neutral hydrogen. For example, interpretation of the *Voyager-1* observations in terms of the classical hot model indicated that the theory disagrees with

[2] Abbreviation from Solar Terrestrial Relations Observatory.

observed results already at a distance of $\sim$ 70 A.U. from the Sun. Theoretical calculations, which have been carried out in the framework of a self-consistent kinetic–gasdynamic model of interaction of the solar wind with a two-component (neutral atoms and plasma) interstellar medium, have shown that the temperature and velocity derived from L_α line observations are not the LISM parameters and most likely relate to distances as small as 40–60 A.U. from the Sun [50, 51]. It was shown that the heliospheric interface starts affecting the velocity distribution of hydrogen atoms already at distances as small as 1–5 A.U. from the Sun.

By the beginning of 2012, *Voyager-1* and *Voyager-2* probes had flown away from the Sun at distances of 18 and 15 bln km, respectively. In April 2010, according to sensors on *Voyager-1*, the solar wind velocity dropped to zero [52, 53], and the magnetic field strength doubled with respect to the value revealed one year earlier [54]; a 100-fold increase in the flux of high-energy electrons was detected. After the middle of 2010, the number of energetic particles emanating from the inner Solar System became half as big as that measured in the previous five years. These can be signatures of an approaching heliopause.

The location of the *Pioneer-10*, *Pioneer-11*, *Voyager-1* and *Voyager-2* space probes as of the beginning of 2012 can be found on the site http://www.heavens-above.com/solar-escape.asp. Also indicated there is the location of the *IBEX* spacecraft launched in 2008 into a high-apogee orbit ($\approx$ 300,000 km above Earth) to explore the physical parameters and structure of the internal shock, as well as interaction processes between the shocks. Two sensors operating in the 0.3–6.0 keV and 0.01–2.00 keV energy ranges are designed to detect high-energy (high-velocity) neutral atoms (Energetic Neutral Atoms — ENAs) that emerge between the shocks. Already the first results have been surprising.

The all-sky map of the spatial distribution of ENAs shows a narrow 'ribbon' $\approx 20°$ wide, which is 2–3 times as bright as the adjacent regions, which was not predicted by any theory [55]. This ribbon is likely to be related to the generation of secondary ENAs in the interstellar magnetic field existing in the LISM [56].

6. Conclusion

The methods described in the present paper allow one to determine parameters of the local interstellar medium only in the immediate vicinity of the Sun, namely beyond the interaction region of the solar wind and LISM. From our point of view, at the present time the most reliable results are of UV observations in the He I line $\lambda = 584$ Å [31] (the velocity and direction of the interstellar wind are determined independently of other parameters) and the related results of direct observations of neutral helium atoms [36]. Thus, the Sun moves relative to the LISM with a velocity of $\sim$ 25–26 km s^{-1}, the ecliptic longitude of the downwind direction is about 75°, and the ecliptic latitude is about $-5°$ (J2000.0). The temperature T_w ranges $\sim 6000-7000$ K. Estimates of the neutral helium density vary within the range of 0.013–0.018 cm^{-3} [17, 32, 57], and the neutral hydrogen density varies from 0.065 to 0.11 cm^{-3} [43, 58]. It is possible that these estimates correspond to the particle number density at the heliospheric shock and do not relate to the LISM.

The work was supported by the Ministry of Education and Science of the Russian Federation under Agreement 8405.

7. Appendix. Absolute calibration of instrumentation for ultraviolet observations

Hydrogen and helium densities, inferred from observations, enter as multipliers into the observed intensity in the optically thin case, which is apparently relevant for both the hydrogen L_α line and the helium line with wavelength $\lambda = 584$ Å. Clearly, the accuracy of the hydrogen and helium density determination depends on the absolute calibration of instruments, i.e., on the response coefficients from instrumental counts given as pulses per second into physical units [erg cm^{-2} s^{-1} sr^{-1}] or rayleigh.[3]

At the initial stage of our measurements in 1961, we calibrated our instruments at the Institute of Astrophysics of the Esthonian AS (Tartu, Tŏravere) using a thermocouple whose sensitivity was independent of the radiation wavelength. In turn, the thermocouple was calibrated against thermal black-body (BB) emission with a temperature of 300–400 K. The calibration error in this many-stage procedure was as high as 100%.

Later on, for the absolute calibration we used two sources, whose intensities can be calculated provided that some parameters are known (BB has only one parameter, the temperature). However, our observations in the vacuum ultraviolet (VUV) range required sources with temperatures as high as 10,000 K or even 20,000 K. Such a source was manufactured by us jointly with the Institute for High Temperatures of RAS using high-pressure gas-filled lamps (for example, filled with xenon). However, the determination of temperature with the required accuracy (of about ± 25 K) is a very complicated task. Clearly, the BB approximation can be applied only in spectral lines, since the hot gas radiation is optically thin in the continuum, and the Planck formula cannot be used. In the continuum, the intensity is almost independent of wavelength, and the emergent spectrum is almost flat. Only in the emission lines is the emission optically thick, and its intensity corresponds to the Planck formula. To arrive at the temperature, we used the determination method of the widths of Balmer lines of hydrogen, which, in small amounts (1–3%), was added to the noble gas in the lamp. This allowed us to estimate the electron density in the lamp, which, in turn, was related to the temperature by the Saha formula. Unfortunately, the absolute calibration error in this method could be as high as 50% due to temperature determination errors. In addition, it was very difficult to take into account the huge radial temperature drop in the gas-discharge tube — from 25,000 K at the discharge axis to 300 K near the water-cooled tube wall.

Synchrotron radiation of relativistic electrons in a magnetic field is another light source with a known absolute intensity. To calculate the intensity of this radiation, the radius of curvature of electron trajectory, magnetic field strength, electron energy, and the number of electrons in the accelerator channel should be specified. We employed the electron–positron VEPP-2M[4] accelerator (energy of electrons amounted to 640 MeV) of the Institute of Nuclear Physics of the Siberian Branch of RAS, to which our group was invited by A M Budker, the Director of the institute at that time. The use of this energy source allowed us to reach an absolute calibration accuracy of 15–20%. In one of the four

[3] 1 rayleigh (R) = 10^6 photons per cm^2 per s per 4π sr.
[4] Colliding Electron–Positron Beams.

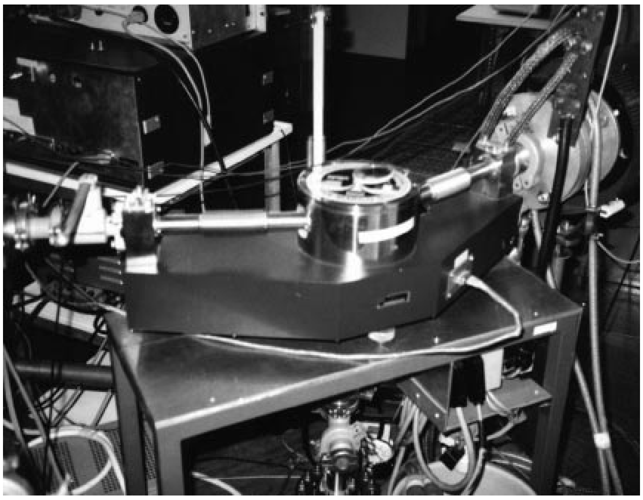

Figure 9. UV vacuum spectrometer for absolute calibration of the payload instrumentation (University of Freiburg, Germany).

channels of the VEPP-2M collider, a normal incidence diffraction spectrometer was mounted. The spectrometer was constructed around the Wadsworth scheme with only one optical element — a convex diffraction grating working in the first order, which was carved onto gold-coated glass, providing the stability of the reflection coefficient of the grating for several years. The transmission coefficient of the spectrometer was determined independently with the aid of a second similar diffraction grating for the dispersed emission behind the first spectrometer. The reflection coefficient of the gold coating in the VUV range is not as high as for pure aluminium, but instead is stable over several years and weakly depends on wavelength in the 1550–300 Å range [59]. Unlike aluminium and silver, gold coatings do not oxidize in air.

At the present time, as well as during our last observations carried out in collaboration with colleagues from France and Germany, the absolute calibration was performed at the University of Freiburg (Germany). A diffraction monochromator (Fig. 9) with one oblique-incidence diffraction grating with a gold coating and a gas-discharge tube filled with H_2, He, Ar, Kr, or Xe were used for this purpose. Different noble gases enabled us to calibrate payload sensors in the wavelength range from 1600 Å to 300 Å. In a vacuum camera, mounted behind the output slot of the monochromator, the registration unit and a standard photodiode were installed, with the latter calibrated against synchrotron radiation at the US National Institute of Standards and Technology (Boulder, Colorado). The instruments could be moved in two perpendicular directions and rotated in the vacuum camera, which allowed both the absolute calibration of the detection unit to be done and the angular dependence of the instrument sensitivity in two perpendicular planes to be measured. The absolute calibration error in this method is estimated to be 10–20%.

Finally, in experiments carried out on the *Prognoz-5* and *Prognoz-6* satellites, we were able to test and improve the calibration using serendipitous observations of bright blue and hot stars in the field of view of the instruments. The spectral energy distribution of such stars is known at present very accurately.

References

1. Morton D C, Dewitt Purcell J *Planet. Space Sci.* **9** 455 (1962)
2. Kurt V G, Dostovalov S B *Nature* **218** 258 (1968)
3. Bertaux J L, Blamont J E *Astron. Astrophys.* **11** 200 (1971)
4. Thomas G E, Krassa R F *Astron. Astrophys.* **11** 218 (1971)
5. Kurt V G, Mironova E N *Phys. Usp.* **55** 825 (2012) [*Usp. Fiz. Nauk* **182** 887 (2012)]
6. Baranov V B, Krasnobaev K V, Kulikovskii A G *Sov. Phys. Dokl.* **15** 791 (1971) [*Dokl. Akad. Nauk SSSR* **194** 41 (1970)]
7. McComas D J et al. *Science* **336** 1291 (2012)
8. Blum P W, Fahr H J *Astron. Astrophys.* **4** 280 (1970)
9. Bertaux J L et al. *Astron. Astrophys.* **150** 1 (1985)
10. Bertaux J L, Lallement R *Astron. Astrophys.* **140** 230 (1984)
11. Vincent F et al., American Geophysical Union, Fall Meeting (2009)
12. Clarke J T et al. *Astrophys. J.* **499** 482 (1998)
13. Quémerais E et al. *Space Sci. Rev.* **143** 151 (2009)
14. Delaboudiniere J P, Carabetian C *Space Sci. Instrum.* **1** 91 (1975)
15. Delaboudiniere J P, Crifo J F, in *Space Research XVI. Proc. of the Open Meetings of Working Groups on Physical Sciences, May 29 – June 7, 1975, and Symp. and Workshop on Results from Coordinated Upper Atmosphere Measurement Programs, Varna, Bulgaria, May 29 – 31, 1975* (Berlin: Akademie-Verlag, 1976) p. 803
16. Fahr H J *Astron. Astrophys.* **14** 263 (1971)
17. Dalaudier F et al. *Astron. Astrophys.* **134** 171 (1984)
18. Lallement R, Bertaux J L, Kurt V G *J. Geophys. Res.* **90** 1413 (1985)
19. Izmodenov V V, Gruntman M, Malama Yu G *J. Geophys. Res.* **106** 10681 (2001)
20. Quémerais E, Izmodenov V *Astron. Astrophys.* **396** 269 (2002)
21. Harris D L (III) *Astrophys. J.* **108** 112 (1948)
22. Bertaux J-L et al. *Space Sci. Rev.* **87** 129 (1999)
23. Quémerais E et al. *J. Geophys. Res.* **104** 12585 (1999)
24. Costa J et al. *Astron. Astrophys.* **349** 660 (1999)
25. Lallement R et al. *AIP Conf. Proc.* **1216** 555 (2010)
26. Paresce F, Bowyer S *Astron. Astrophys.* **27** 399 (1973)
27. Paresce F, Bowyer S, Kumar S *Astrophys. J.* **183** L87 (1973)
28. Weller C S, Meier R R *Astrophys. J.* **193** 471 (1974)
29. Ajello J M *Astrophys. J.* **222** 1068 (1978)
30. Broadfoot A L, Kumar S *Astrophys. J.* **222** 1054 (1978)
31. Kurt V G et al. *Kosmich. Issled.* **22** 97 (1984)
32. Vallerga J et al. *Astron. Astrophys.* **426** 855 (2004)
33. Blum P W, Pfleiderer J, Wulf-Mathies C *Planet. Space Sci.* **23** 93 (1975)
34. Witte M et al. *Astron. Astrophys. Suppl.* **92** 333 (1992)
35. Witte M, Banaszkiewicz M, Rosenbauer H *Space Sci. Rev.* **78** 289 (1996)
36. Banaszkiewicz M, Witte M, Rosenbauer H *Astron. Astrophys. Suppl.* **120** 587 (1996)
37. Fuselier S A et al. *Space Sci. Rev.* **146** 117 (2009)
38. Bzowski M et al., American Geophysical Union, Fall Meeting (2010), abstract #SH21A-1791
39. Bzowski M et al. *Astrophys. J. Suppl.* **198** 12 (2012)
40. Moebius E et al., American Geophysical Union, Fall Meeting (2010), abstract #SH23D-08
41. Moebius E et al. *Astron. Astrophys.* **304** 505 (1995)
42. Gloeckler G et al. *Astron. Astrophys.* **426** 845 (2004)
43. Kallenbach R et al. *Astron. Space Sci.* **274** 97 (2000)
44. Möbius E et al. *J. Geophys. Res.* **103** 257 (1998)
45. Stone E C et al. *Nature* **454** 71 (2008)
46. Izmodenov V V, Alexashov D, Myasnikov A *Astron. Astrophys.* **437** L35 (2005)
47. Izmodenov V V *Space Sci. Rev.* **143** 139 (2009)
48. Wang L et al. *Nature* **454** 81 (2008)
49. Wang L, American Geophysical Union, Fall Meeting (2008), abstract #SH14A-05
50. Baranov V B, Malama Yu G *J. Geophys. Res.* **98** 15157 (1993)
51. Katushkina O A, Izmodenov V V *Adv. Space Res.* **48** 1967 (2011)
52. Krimigis S M et al. *Nature* **474** 359 (2011)
53. Decker R B et al. *Nature* **489** 124 (2012)
54. Burlaga L F, Ness N F *Astrophys J.* **749** 13 (2012)
55. McComas D J et al. *Science* **326** 959 (2009)
56. Chalov S V et al. *Astrophys. J. Lett.* **716** L99 (2010)
57. Chassefiere E et al. *Astron. Astrophys.* **160** 229 (1986)
58. Bertaux J-L et al. *Kosmich. Issled.* **22** 91 (1984)
59. Samson J A R *Techniques of Vacuum Ultraviolet Spectroscopy* (New York: Wiley, 1967)